The Astrophysical Journal, 952:91 (11pp), 2023 July 20 https://doi.org/10.3847/1538-4357/acc862

Search for Ultra-high-energy Photons from Gravitational Wave Sources with the Pierre Auger Observatory

A. Abdul Halim[1], P. Abreu[2], M. Aglietta[3,4], I. Allekotte[5], K. Almeida Cheminant[6], A. Almela[7,8], J. Alvarez-Muñiz[9], J. Ammerman Yebra[9], G. A. Anastasi[3,4], L. Anchordoqui[10], B. Andrada[7], S. Andringa[2], C. Aramo[11], P. R. Araújo Ferreira[12], E. Arnone[13,4], J. C. Arteaga Velázquez[14], H. Asorey[7], P. Assis[2], G. Avila[15], E. Avocone[16,17], A. M. Badescu[18], A. Bakalova[19], A. Balaceanu[20], F. Barbato[21,17], J. A. Bellido[1,22], C. Berat[23], M. E. Bertaina[4,13], G. Bhatta[6], P. L. Biermann[24,92], V. Binet[24], K. Bismark[25,7], T. Bister[12], J. Biteau[26], J. Blazek[19], C. Bleve[23], J. Blümer[27], M. Boháčová[19], D. Boncioli[16,17], C. Bonifazi[28,29], L. Bonneau Arbeletche[30], N. Borodai[6], J. Brack[14,93], T. Bretz[12], P. G. Brichetto Orchera[7], F. L. Briechle[12], P. Buchholz[31], A. Bueno[32], S. Buitink[33], M. Buscemi[34,35], M. Büsken[25,7], A. Bwembya[36,37], K. S. Caballero-Mora[38], L. Caccianiga[39,40], I. Caracas[41], R. Caruso[34,42], A. Castellina[3,4], F. Catalani[43], G. Cataldi[44], L. Cazon[9], M. Cerda[45], J. A. Chinellato[30], J. Chudoba[19], L. Chytka[46], R. W. Clay[1], A. C. Cobos Cerutti[47], R. Colalillo[48,11], A. Coleman[49], M. R. Coluccia[44], R. Conceiçao[2], A. Condorelli[26], G. Consolati[40,50], M. Conte[51,44], F. Contreras[15], F. Convenga[27], D. Correia dos Santos[52], P. J. Costa[2], C. E. Covault[53], M. Cristinziani[31], C. S. Cruz Sanchez[54], S. Dasso[55,56], K. Daumiller[27], B. R. Dawson[1], R. M. de Almeida[52], J. de Jesús[7,27], S. J. de Jong[36,37], J. R. T. de Mello Neto[29,57], I. De Mitri[21,17], J. de Oliveira[58], D. de Oliveira Franco[30], F. de Palma[44,51], V. de Souza[59], E. De Vito[51,44], A. Del Popolo[42,34], O. Deligny[60], L. Deval[27,7], A. di Matteo[4], M. Dobre[20], C. Dobrigkeit[30], J. C. D'Olivo[61], L. M. Domingues Mendes[2], R. C. dos Anjos[62], J. Ebr[19], M. Emam[36,37], R. Engel[25,27], I. Epicoco[51,44], M. Erdmann[12], A. Etchegoyen[7,8], H. Falcke[36,63,37], J. Farmer[64], G. Farrar[65], A. C. Fauth[30], N. Fazzini[66,94], F. Feldbusch[66], F. Fenu[27], A. Fernandes[2], B. Fick[67], J. M. Figueira[7], A. Filipčič[68,69], T. Fitoussi[27], B. Flaggs[49], T. Fodran[36], T. Fujii[64,95], A. Fuster[7,8], C. Galea[36], C. Galelli[39,40], B. García[47], H. Gemmeke[66], F. Gesualdi[7,27], A. Gherghel-Lascu[20], P. L. Ghia[60], U. Giaccari[44], M. Giammarchi[40], J. Glombitza[27,96], F. Gobbi[45], F. Gollan[7], G. Golup[5], M. Gómez Berisso[5], P. F. Gómez Vitale[15], J. P. Gongora[15], J. M. González[5], N. González[70], I. Goos[5], D. Góra[6], A. Gorgi[3,4], M. Gottowik[9], T. D. Grubb[1], F. Guarino[48,11], G. P. Guedes[71], E. Guido[31], S. Hahn[27,7], P. Hamal[19], M. R. Hampel[7], P. Hansen[54], D. Harari[5], V. M. Harvey[1], A. Haungs[27], T. Hebbeker[12], D. Heck[27], C. Hojvat[36,37,94], J. R. Hörandel[36,37], P. Horvath[46], M. Hrabovský[46], T. Huege[27,33], A. Insolia[42,34], P. G. Isar[72], P. Janecek[19], J. A. Johnsen[73], J. Jurysek[19], A. Kääpä[41], K. H. Kampert[41], B. Keilhauer[27], A. Khakurdikar[36], V. V. Kizakke Covilakam[7,27], H. O. Klages[27], M. Kleifges[66], J. Kleinfeller[45], F. Knapp[25], N. Kunka[66], B. L. Lago[74], N. Langner[12], M. A. Leigui de Oliveira[75], V. Lenok[25], A. Letessier-Selvon[76], I. Lhenry-Yvon[60], D. Lo Presti[42,34], L. Lopes[2], R. López[77], L. Lu[78], Q. Luce[25], J. P. Lundquist[69], A. Machado Payeras[30], M. Majercakova[19], D. Mandat[19], B. C. Manning[1], J. Manshanden[79], P. Mantsch[60,94], S. Marafico[60], F. M. Mariani[39,40], A. G. Mariazzi[54], I. C. Mariş[70], G. Marsella[35,34], D. Martello[44,51], S. Martinelli[27,7], O. Martínez Bravo[77], M. A. Martins[9], M. Mastrodicasa[16,17], H. J. Mathes[27], J. Matthews[80,81,97], G. Matthiae[80,81], E. Mayotte[73,41], S. Mayotte[73], P. O. Mazur[61,94], G. Medina-Tanco[61], J. Meinert[41], D. Melo[7], A. Menshikov[66], S. Michal[46], M. I. Micheletti[24], L. Miramonti[39,40], S. Mollerach[5], F. Montanet[23], L. Morejon[41], C. Morello[3,4], A. L. Müller[19], K. Mulrey[36,37], R. Mussa[4], M. Muzio[65], W. M. Namasaka[41], A. Nasr-Esfahani[41], L. Nellen[61], G. Nicora[82], M. Niculescu-Oglinzanu[20], M. Niechciol[31], D. Nitz[67], I. Norwood[67], D. Nosek[83], V. Novotny[83], L. Nožka[46], A. Nucita[44,51], L. A. Núñez[84], C. Oliveira[59], M. Palatka[19], J. Pallotta[82], G. Parente[9], A. Parra[77], J. Pawlowsky[41], M. Pech[19], J. Pękala[6], R. Pelayo[85], L. A. S. Pereira[86], E. E. Pereira Martins[25,7], J. Perez Armand[87], C. Pérez Bertolli[7,27], L. Perrone[51,44], S. Petrera[21,17], C. Petrucci[16,17], T. Pierog[27], M. Pimenta[2], M. Platino[7], B. Pont[36], M. Pothast[37,36], M. Pourmohammad Shavar[35,34], P. Privitera[64], M. Prouza[19], A. Puyleart[67], S. Querchfeld[41], J. Rautenberg[41], D. Ravignani[7], M. Reininghaus[25], J. Ridky[19], F. Riehn[9], M. Risse[31], V. Rizi[16,17], W. Rodrigues de Carvalho[36], J. Rodriguez Rojo[15], M. J. Roncoroni[7], S. Rossoni[79], M. Roth[27], E. Roulet[5], A. C. Rovero[55], P. Ruehl[31], A. Saftoiu[20], M. Saharan[36], F. Salamida[16,17], H. Salazar[77], G. Salina[81], J. D. Sanabria Gomez[84], F. Sánchez[7], E. M. Santos[87], E. Santos[19], F. Sarazin[73], R. Sarmento[2], R. Sato[15], P. Savina[78], C. M. Schäfer[27], V. Scherini[51,44], H. Schieler[27], M. Schimassek[60], M. Schimp[41], F. Schlüter[27], D. Schmidt[25], O. Scholten[33], H. Schoorlemmer[36,37], P. Schovánek[19], F. G. Schröder[49,27], J. Schulte[12], T. Schulz[27], S. J. Sciutto[54], M. Scornavacche[7,27], A. Segreto[88,34], S. Sehgal[41], S. U. Shivashankara[69], G. Sigl[79], G. Silli[7], O. Sima[20,98], R. Smau[20], R. Šmída[64], P. Sommers[10,99], J. F. Soriano[10], R. Squartini[45], M. Stadelmaier[19], D. Stanca[20], S. Stanič[69], J. Stasielak[6], P. Stassi[23], M. Straub[12], A. Streich[25,7], M. Suárez-Durán[70], T. Suomijärvi[26], A. D. Supanitsky[7], Z. Szadkowski[89], A. Tapia[90], C. Taricco[13,4], C. Timmermans[37,36], O. Tkachenko[27], P. Tobiska[19], C. J. Todero Peixoto[43], B. Tomé[2], Z. Torrès[23], A. Travaini[45], P. Travnicek[19], C. Trimarelli[16,17], M. Tueros[54], R. Ulrich[27], M. Unger[27], L. Vaclavek[46], M. Vacula[46], J. F. Valdés Galicia[61], L. Valore[48,11], E. Varela[77], A. Vásquez-Ramírez[84], D. Veberič[27], C. Ventura[57], I. D. Vergara Quispe[54], V. Verzi[81], J. Vicha[19], J. Vink[91], S. Vorobiov[69], C. Watanabe[29], A. A. Watson[27,100], A. Weindl[27], L. Wiencke[73], H. Wilczyński[6], D. Wittkowski[41], B. Wundheiler[7], A. Yushkov[19], O. Zapparrata[70], E. Zas[9], D. Zavrtanik[69,68], and M. Zavrtanik[68,69]
The Pierre Auger Collaboration

[1] University of Adelaide, Adelaide, SA, Australia; spokespersons@auger.org
[2] Laboratório de Instrumentaçao e Física Experimental de Partículas—LIP and Instituto Superior Técnico—IST, Universidade de Lisboa—UL, Lisboa, Portugal
[3] Osservatorio Astrofisico di Torino (INAF), Torino, Italy

[4] INFN, Sezione di Torino, Torino, Italy
[5] Centro Atómico Bariloche and Instituto Balseiro (CNEA-UNCuyo-CONICET), San Carlos de Bariloche, Argentina
[6] Institute of Nuclear Physics PAN, Krakow, Poland
[7] Instituto de Tecnologías en Detección y Astropartículas (CNEA, CONICET, UNSAM), Buenos Aires, Argentina
[8] Universidad Tecnológica Nacional—Facultad Regional Buenos Aires, Buenos Aires, Argentina
[9] Instituto Galego de Física de Altas Enerxías (IGFAE), Universidade de Santiago de Compostela, Santiago de Compostela, Spain
[10] Department of Physics and Astronomy, Lehman College, City University of New York, Bronx, NY, USA
[11] INFN, Sezione di Napoli, Napoli, Italy
[12] III. Physikalisches Institut A, RWTH Aachen University, Aachen, Germany
[13] Dipartimento di Fisica, Università Torino, Torino, Italy
[14] Universidad Michoacana de San Nicolás de Hidalgo, Morelia, Michoacán, México
[15] Observatorio Pierre Auger and Comisión Nacional de Energía Atómica, Malargüe, Argentina
[16] Dipartimento di Scienze Fisiche e Chimiche, Università dell'Aquila, L'Aquila, Italy
[17] INFN Laboratori Nazionali del Gran Sasso, Assergi (L'Aquila), Italy
[18] University Politehnica of Bucharest, Bucharest, Romania
[19] Institute of Physics of the Czech Academy of Sciences, Prague, Czech Republic
[20] "Horia Hulubei" National Institute for Physics and Nuclear Engineering, Bucharest-Magurele, Romania
[21] Gran Sasso Science Institute, L'Aquila, Italy
[22] Facultad de Ciencias Naturales y Formales, Universidad Nacional de San Agustin de Arequipa, Arequipa, Peru
[23] Grenoble Institute of Engineering, Univ. Grenoble Alpes, CNRS, LPSC-IN2P3, F-38000 Grenoble, France
[24] Instituto de Física de Rosario (IFIR)—CONICET/U.N.R. and Facultad de Ciencias Bioquímicas y Farmacéuticas U.N.R., Rosario, Argentina
[25] Institute for Experimental Particle Physics, Karlsruhe Institute of Technology (KIT), Karlsruhe, Germany
[26] Université Paris-Saclay, CNRS/IN2P3, IJCLab, Orsay, France
[27] Institute for Astroparticle Physics, Karlsruhe Institute of Technology (KIT), Karlsruhe, Germany
[28] International Center of Advanced Studies and Instituto de Ciencias Físicas, ECyT-UNSAM and CONICET, Campus Miguelete—San Martín, Buenos Aires, Argentina
[29] Instituto de Física, Universidade Federal do Rio de Janeiro, Rio de Janeiro, RJ, Brazil
[30] Universidade Estadual de Campinas, IFGW, Campinas, SP, Brazil
[31] Department Physik—Experimentelle Teilchenphysik, Universität Siegen, Siegen, Germany
[32] Universidad de Granada and C.A.F.P.E., Granada, Spain
[33] Vrije Universiteit Brussels, Brussels, Belgium
[34] INFN, Sezione di Catania, Catania, Italy
[35] Dipartimento di Fisica e Chimica "E. Segrè", Università di Palermo, Palermo, Italy
[36] IMAPP, Radboud University Nijmegen, Nijmegen, The Netherlands
[37] Nationaal Instituut voor Kernfysica en Hoge Energie Fysica (NIKHEF), Science Park, Amsterdam, The Netherlands
[38] Universidad Autónoma de Chiapas, Tuxtla Gutiérrez, Chiapas, México
[39] Dipartimento di Fisica, Università di Milano, Milano, Italy
[40] INFN, Sezione di Milano, Milano, Italy
[41] Department of Physics, Bergische Universität Wuppertal, Wuppertal, Germany
[42] Dipartimento di Fisica e Astronomia "Ettore Majorana", Università di Catania, Catania, Italy
[43] Escola de Engenharia de Lorena, Universidade de São Paulo, Lorena, SP, Brazil
[44] INFN, Sezione di Lecce, Lecce, Italy
[45] Observatorio Pierre Auger, Malargüe, Argentina
[46] Palacky University, Olomouc, Czech Republic
[47] Instituto de Tecnologías en Detección y Astropartículas (CNEA, CONICET, UNSAM), and Universidad Tecnológica Nacional—Facultad Regional Mendoza (CONICET/CNEA), Mendoza, Argentina
[48] Dipartimento di Fisica "Ettore Pancini", Università di Napoli "Federico II", Napoli, Italy
[49] Department of Physics and Astronomy, Bartol Research Institute, University of Delaware, Newark, DE, USA
[50] Politecnico di Milano, Dipartimento di Scienze e Tecnologie Aerospaziali, Milano, Italy
[51] Dipartimento di Matematica e Fisica "E. De Giorgi", Università del Salento, Lecce, Italy
[52] Universidade Federal Fluminense, EEIMVR, Volta Redonda, RJ, Brazil
[53] Case Western Reserve University, Cleveland, OH, USA
[54] IFLP, Universidad Nacional de La Plata and CONICET, La Plata, Argentina
[55] Instituto de Astronomía y Física del Espacio (IAFE, CONICET-UBA), Buenos Aires, Argentina
[56] Departamento de Física and Departamento de Ciencias de la Atmósfera y los Océanos, FCEyN, Universidad de Buenos Aires and CONICET, Buenos Aires, Argentina
[57] Universidade Federal do Rio de Janeiro (UFRJ), Observatório do Valongo, Rio de Janeiro, RJ, Brazil
[58] Instituto Federal de Educaçao, Ciência e Tecnologia do Rio de Janeiro (IFRJ), Brazil
[59] Instituto de Física de Sao Carlos, Universidade de São Paulo, Sao Carlos, SP, Brazil
[60] CNRS/IN2P3, IJCLab, Université Paris-Saclay, Orsay, France
[61] Universidad Nacional Autónoma de México, México, D.F., México
[62] Universidade Federal do Paraná, Setor Palotina, Palotina, Brazil
[63] Stichting Astronomisch Onderzoek in Nederland (ASTRON), Dwingeloo, The Netherlands
[64] Enrico Fermi Institute, University of Chicago, Chicago, IL, USA
[65] New York University, New York, NY, USA
[66] Institut für Prozessdatenverarbeitung und Elektronik, Karlsruhe Institute of Technology (KIT), Karlsruhe, Germany
[67] Michigan Technological University, Houghton, MI, USA
[68] Experimental Particle Physics Department, J. Stefan Institute, Ljubljana, Slovenia
[69] Center for Astrophysics and Cosmology (CAC), University of Nova Gorica, Nova Gorica, Slovenia
[70] Université Libre de Bruxelles (ULB), Brussels, Belgium
[71] Universidade Estadual de Feira de Santana, Feira de Santana, Brazil
[72] Institute of Space Science, Bucharest-Magurele, Romania
[73] Colorado School of Mines, Golden, CO, USA
[74] Centro Federal de Educaçao Tecnológica Celso Suckow da Fonseca, Petropolis, Brazil
[75] Universidade Federal do ABC, Santo André, SP, Brazil
[76] Laboratoire de Physique Nucléaire et de Hautes Energies (LPNHE), Sorbonne Université, Université de Paris, CNRS-IN2P3, Paris, France

[77] Benemérita Universidad Autónoma de Puebla, Puebla, México
[78] Department of Physics and WIPAC, University of Wisconsin-Madison, Madison, WI, USA
[79] II. Institut für Theoretische Physik, Universität Hamburg, Hamburg, Germany
[80] Dipartimento di Fisica, Università di Roma "Tor Vergata", Roma, Italy
[81] INFN, Sezione di Roma "Tor Vergata", Roma, Italy
[82] Centro de Investigaciones en Láseres y Aplicaciones, CITEDEF and CONICET, Villa Martelli, Argentina
[83] Faculty of Mathematics and Physics, Institute of Particle and Nuclear Physics, Charles University, Prague, Czech Republic
[84] Universidad Industrial de Santander, Bucaramanga, Colombia
[85] Unidad Profesional Interdisciplinaria en Ingeniería y Tecnologías Avanzadas del Instituto Politécnico Nacional (UPIITA-IPN), México, D.F., México
[86] Centro de Ciencias e Tecnologia, Universidade Federal de Campina Grande, Campina Grande, Brazil
[87] Instituto de Física, Universidade de São Paulo, São Paulo, SP, Brazil
[88] Istituto di Astrofisica Spaziale e Fisica Cosmica di Palermo (INAF), Palermo, Italy
[89] Faculty of High-Energy Astrophysics, University of Łódź, Łódź, Poland
[90] Universidad de Medellín, Medellín, Colombia
[91] Faculty of Science, Universiteit van Amsterdam, Amsterdam, The Netherlands
Received 2022 December 14; revised 2023 March 19; accepted 2023 March 27; published 2023 July 19

Abstract

A search for time-directional coincidences of ultra-high-energy (UHE) photons above 10 EeV with gravitational wave (GW) events from the LIGO/Virgo runs O1 to O3 is conducted with the Pierre Auger Observatory. Due to the distinctive properties of photon interactions and to the background expected from hadronic showers, a subset of the most interesting GW events is selected based on their localization quality and distance. Time periods of 1000 s around and 1 day after the GW events are analyzed. No coincidences are observed. Upper limits on the UHE photon fluence from a GW event are derived that are typically at $\sim 7\,\mathrm{MeV\,cm^{-2}}$ (time period 1000 s) and $\sim 35\,\mathrm{MeV\,cm^{-2}}$ (time period 1 day). Due to the proximity of the binary neutron star merger GW170817, the energy of the source transferred into UHE photons above 40 EeV is constrained to be less than 20% of its total GW energy. These are the first limits on UHE photons from GW sources.

Unified Astronomy Thesaurus concepts: Particle astrophysics (96); Ultra-high-energy cosmic radiation (1733); Cosmic ray showers (327); Gravitational wave sources (677); Transient sources (1851)

1. Introduction

With the first gravitational waves (GWs) measured by the Advanced LIGO and Virgo detectors in 2015 (Abbott et al. 2016), a new window to the universe has been opened. In addition, a new type of transient astronomical object has been observed for the first time: the merging process of two compact stellar-mass objects (a compact binary merger, CBM). Since the first measurement in 2015, three observation runs (O1, O2, and O3) have been conducted with a total yield of 91 confident GW observations. The sources of these signals turned out to belong to different groups, including the merging events of binary black holes (BBHs), binary neutron stars (BNSs), and neutron star–black hole (NSBH) systems (Abbott et al. 2019, 2021a, 2021b, 2021c).

An extensive follow-up campaign in the electromagnetic domain revealed a coincident kilonova event from the BNS merger GW170817, whereas no astrophysical neutrino signal has been identified (Abbott et al. 2017). This observation became a milestone of multimessenger astronomy and the first multimessenger observation involving GWs. The acceleration mechanisms of cosmic rays for such an event are being debated in the theoretical community (Fang & Metzger 2017; Kimura et al. 2018; Rodrigues et al. 2019; Decoene et al. 2020). Although no further observations of electromagnetic or neutrino counterparts from other GW sources have been confirmed so far, BBH and NSBH mergers are also being discussed as possible candidates for the acceleration of ultra-high-energy (UHE) cosmic rays and, hence, potential sources of high-energy neutrinos and photons (Kotera & Silk 2016; Murase et al. 2016; McKernan et al. 2019).

With its design sensitivity at the highest energies in the cosmic ray spectrum above 10^{18} eV, the Pierre Auger Observatory (Aab et al. 2015) plays an important role in the multimessenger follow-up campaign of GW sources (Kampert et al. 2019). Constraints on the production of UHE neutrinos by the source of GW170817 and the first BBH mergers detected during O1 have been obtained (Aab et al. 2016; Albert et al. 2017), and a stacking analysis has been performed using 83 confident BBH merger observations aiming to constrain the neutrino emission from the source class as a whole (A. Abdul Halim et al. 2023, in preparation). A first analysis of GW sources with respect to an UHE photon signal using the data of the Pierre Auger Observatory is reported here. Although the attenuation length of UHE photons is of the order of 10 Mpc due to interactions with the cosmic background radiation fields (Risse & Homola 2007)—mainly the cosmic microwave background and the universal radio background—it turns out that the exposure of the Pierre Auger Observatory toward UHE photons is large enough to potentially observe photons from sufficiently close sources. More distant sources, on the other hand, can be used to probe the attenuation of UHE photons in

[92] Max-Planck-Institut für Radioastronomie, Bonn, Germany.
[93] Colorado State University, Fort Collins, CO, USA.
[94] Fermi National Accelerator Laboratory, Fermilab, Batavia, IL, USA.
[95] Now at Graduate School of Science, Osaka Metropolitan University, Osaka, Japan.
[96] Now at ECAP, Erlangen, Germany.
[97] Louisiana State University, Baton Rouge, LA, USA.
[98] Also at University of Bucharest, Physics Department, Bucharest, Romania.
[99] Pennsylvania State University, University Park, PA, USA.
[100] School of Physics and Astronomy, University of Leeds, Leeds, UK.

the background radiation fields, and an observation of an UHE photon from such a source could point to new physics scenarios (Galaverni & Sigl 2008; Fairbairn et al. 2011). Focusing on the most promising sources while keeping an open window for unexpected discovery, a selected set of GW sources will be analyzed here to reduce the overall background from hadronic cosmic rays.

The paper is structured as follows. In Section 2, a summary of the method used to search for UHE photons with the Pierre Auger Observatory is provided. In Section 3, an overview of the already concluded GW observation runs and the GW data relevant for this work is given. A description of the GW selection strategy that is used to pick only the most relevant GW sources is detailed in Section 4, followed by a brief discussion in Section 5 of the signal sensitivity that can be achieved using that selection. The final results of the analysis are presented in Section 6 in the form of upper limits on UHE photons from this selection of sources. Section 7 concludes with a short summary and a comparison of our results to other search results from the literature.

2. Ultra-high-energy Photon Search at the Auger Observatory

The search for an UHE photon signal in coincidence with a GW is carried out using data collected by the surface detector array (SD) of the Pierre Auger Observatory (Aab et al. 2015). The SD consists of 1660 autonomous water Cherenkov detectors (WCDs) arranged on a triangular grid with a spacing of 1500 m. Its geolocation is at -69.0° in longitude and -35.4° in latitude, in the western part of Argentina. With a field of view to UHE photons limited to the zenith-angle range between 30° and 60° (as determined by data quality cuts necessary for the photon identification method used), a fraction of 18.3% of the whole sky is covered at any time. Due the field of view and the geolocation of the observatory, 70.8% of the sky is covered during a full rotation of the Earth. A small region with a radius of about 5° around the celestial south pole is constantly observed.

The bulk of data received at the Pierre Auger Observatory originates from cosmic rays of hadronic nature. With its different detector components and various enhancements, the observatory is also sensitive to a possible component of primary photons. Different searches have been performed aiming to identify such a component among the diffuse flux of cosmic rays (Aab et al. 2017a; Abreu et al. 2023, 2022), as well as from steady point sources in the sky (Aab et al. 2017b). No statistically significant excess of primary UHE photons has been identified so far, and the strongest constraints to date on the flux of photons from 2×10^{17} eV up to energies beyond 10^{20} eV have been obtained.

If an air-shower event in coincidence with a GW is found, a method is needed to judge the likelihood of it originating from a primary photon or hadron. For this purpose, the photon-discrimination method from Abreu et al. (2023) is adopted, which is briefly described in the following. This method utilizes the data recorded by the SD taking advantage of its high duty cycle of almost 100%. The identification of photon-induced air showers is based on the shower lateral distribution, i.e., the distribution of particles as a function of the distance to the shower axis, and the shapes of the signal time traces recorded by the WCD stations. In particular, two discriminating photon observables are used, termed $L_{\rm LDF}$ and Δ. Photon-induced air showers, which are typically poor in muons, show on average a steeper lateral distribution function (LDF) compared to hadron-induced showers. The observable $L_{\rm LDF}$ measures the signal in the WCDs as a function of their distance to the shower axis and is therefore sensitive to the steepness of the LDF. The second observable, Δ, quantifies the deviation of the rise time from a reference signal, typical of hadron-induced showers as measured in data. It is sensitive to both the ratio between the electromagnetic and the muonic shower components at the ground level, and to $X_{\rm max}$, which is the atmospheric depth (slant depth) where the shower reaches its maximum development. Photon-induced air showers are expected to exhibit a large deviation from the average (hadronic) data, i.e., large Δ, because their signal rise time will be longer due to an intrinsically smaller muonic component and a less attenuated electromagnetic component (as a consequence of a deeper $X_{\rm max}$). To maximize the photon–hadron separation power, the observables are first normalized with respect to the total signal and the direction of the shower axis and are then combined using a Fisher discriminant analysis. The distributions of the Fisher discriminant of data events and a set of simulated photon events are shown in Figure 1. A typical photon-induced air shower is expected to have a significantly larger Fisher discriminant value than the average event found in data. The distributions shown in Figure 1 provide a measure with which to judge the likelihood of a single event originating from a primary photon.

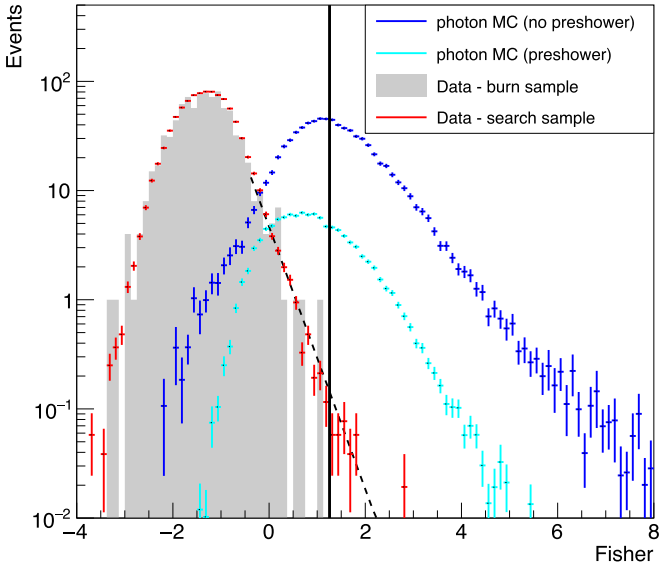

Figure 1. Distributions of the Fisher discriminant values of a set of simulated photon events (blue) and data events (red) with photon energies above 10^{19} eV recorded by the SD (Abreu et al. 2023). The dark blue distribution shows the subset of photon simulations which did not initiate a preshower, i.e., did not interact in the geomagnetic field before reaching the atmosphere, while the light blue distribution displays preshower events exclusively. This subset was used in Abreu et al. (2023) to derive the photon cut above which an event can be regarded as a photon candidate (black vertical line). The right tail of the data distribution has been fitted by an exponential function (tilted black line) to compare the number of observed events passing the cut value with the expectation. The search sample and the photon distributions are scaled so as to have the same integral as the burn sample one (gray).

On the axis of the Fisher discriminant, a threshold value may be placed to define which events will be accepted as "photon candidate events." Depending on this photon candidate selection cut, the photon-discrimination method described above has a nonzero rate of expected false-positive detections

contributing a certain amount of background within the signal region. In Abreu et al. (2023), out of all air-shower events recorded during a period of 16.5 yr (2004 January–2020 June), 16 events passed the photon candidate cut, which was placed at the median of the distribution of photon simulations in that analysis (see vertical line in Figure 1). This number was found to be consistent with the expected hadronic background.

The photon-discrimination method is optimized for air showers with incident zenith angles θ between 30° and 60° and photon energies $E_\gamma > 10^{19}$ eV. Since the energy scale of the SD is calibrated using hadronic air showers observed by both the SD and the fluorescence detectors, the energy of a possible photon-induced air shower would be underestimated. In order to obtain a less biased estimator for the photon energy E_γ, the hadronic energy scale has been replaced by a function of $S(1000)$ and θ calibrated with photon simulations (Abreu et al. 2023). Here, $S(1000)$ is the interpolated average signal produced in an SD station with a perpendicular distance of 1000 m from the shower axis. The photon energy estimator E_γ can be calculated for any air shower with reconstructed $S(1000)$ and zenith angle, and is used to define the lower-energy cut for the application of the analysis.

To clean the shower data set of non-well-reconstructed events, a number of selection criteria is imposed prior to the calculation of the discriminating air-shower observables. The selected events are required to have a successfully reconstructed shower axis and LDF, and have to fulfill the 6T5 trigger criterion (= six active SD stations around the station with the highest signal). For the calculation of Δ and $L_{\rm LDF}$, events with reconstructed hadronic energy $E_{\rm hd} < 10^{18}$ eV (energy estimator obtained by the standard SD energy reconstruction; Aab et al. 2015), and events without triggered stations (excluding stations with a saturated low-gain channel) more than 1000 m away from the shower axis are rejected. A more detailed description of the two observables, $L_{\rm LDF}$ and Δ, and further details of the photon–hadron separation method can be found in Abreu et al. (2023).

3. Gravitational Wave Data

The GW events considered in this analysis were recorded by the Advanced LIGO and Virgo detectors during their first three observation runs and published in three GW transient catalogs: GWTC-1 (Abbott et al. 2019), GWTC-2 (Abbott et al. 2021a) with its second revision GWTC-2.1 (Abbott et al. 2021b), and GWTC-3 (Abbott et al. 2021c). While the first catalog covers the observations of the first two runs O1 (from 2015 September 12 to 2016 January 19) and O2 (from 2016 November 30 to 2017 August 25), the third observation run has been split in two parts, O3a (from 2019 April 1 to 2019 October 1) and O3b (from 2019 November 1 to 2020 March 27), with a maintenance break of 1 month in between. The observations of each part of O3 have been released in separate catalogs, GWTC-2 (GWTC-2.1) and GWTC-3, respectively.

The key information about GWs which is important for this analysis is the localization of their sources. This information is distributed by the GW observatories in the form of probability density distributions realized via pixelized sky maps ("localization maps") in the HEALPix (Gorski et al. 2005) segmentation scheme. The resolution of these maps varies between GW events and typically depends on the overall localization quality of a source. In addition to the directional localization, a "best-fit" estimator for the luminosity distance $D_{\rm L}$ is also given for each source. In the case of GW170817, additional information about the host galaxy, NGC 4993, is available. In this case, the source is treated as a point source and the well-constrained distance to the host galaxy is used instead of the estimate provided by the GW measurement. The pronounced differences in localization qualities and distances give rise to a priorization of sources in the context of this analysis.

4. Gravitational Wave Event Selection

Due to shower-to-shower fluctuations, photon-induced air showers cannot unambiguously be separated from the bulk of showers with hadronic origin. Since the 16 photon candidate events found in Abreu et al. (2023) are consistent with the expected hadronic background, this number may serve as an estimate of the background rate for the present analysis. This leads to a directional-averaged background rate of $\beta_{\rm cand} = (1.86^{+0.58}_{-0.45}) \times 10^{-21}\,{\rm cm^{-2}\,s^{-1}\,sr^{-1}}$. With this rate, the expected number of background events passing the photon candidate cut from all 91 GW sources for a 1 day search period within the 90% localization regions is $b = 0.017$. Hence, the background hypothesis could only be rejected at a level of 1.67σ (derived using the Feldman–Cousins method described in the following paragraph), should a coincident shower with a Fisher discriminant above the photon median be detected. Hence, an actual photon event could not be identified as such and had to be attributed to the hadronic background because of the high background rate. Possible ways to reduce the total background for a set of GW events include a reduction of the temporal and directional search windows. With an additional selection of GW events, the background contamination of the search regions can further be efficiently reduced, boosting the sensitivity of the analysis.

The sensitivity to a possible signal of primary photons can be quantified through the confidence level (CL) at which the background hypothesis can be rejected in the case of a detection. For a given number of observed photon candidate events and a given background, two-sided confidence intervals for the true expectation value can be obtained through the construction described by Feldman & Cousins (1998, hereafter FC). Depending on the CL, the lower limit of this interval may or may not be equal to zero. Thus, as a convenient measure for the sensitivity, we define $\bar{P}_{\rm bg}$ as the lowest CL at which the lower FC limit is still consistent with zero for the given background and a measured number of one photon candidate event. Technically, this is done by calculating the FC confidence interval for a given background b (i.e., the expected number of coincident air-shower events not associated with a transient event) and an assumed signal $s = 1$ (i.e., the number of actual photon events originating from a particular transient) and iterating through the CL until the lower limit matches exactly 0, i.e., so that a slightly lower CL would lead to a lower limit >0. With this definition, $\bar{P}_{\rm bg}$ only depends on b and, naturally, a higher number of expected background events leads to a lower value of $\bar{P}_{\rm bg}$—the CL at which the hypothesis of a photon candidate belonging to the hadronic background can be rejected.

In the following, the term "photon candidate event" shall be used for air-shower events with a Fisher discriminant value larger than the photon candidate cut value used in Abreu et al. (2023). However, for this analysis, this value is only relevant for the definition of the GW selection strategy described in the following. The likelihood of an air-shower event that coincides

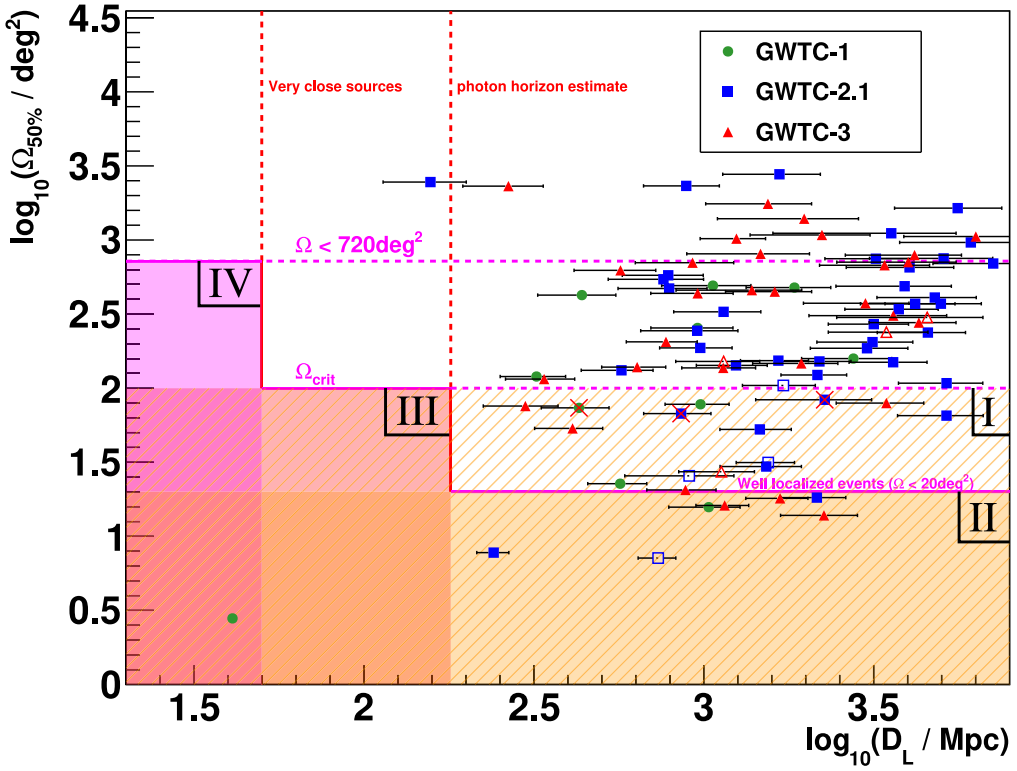

Figure 2. All GW events from GWTC-1 (green dots), GWTC-2.1 (blue squares), and GWTC-3 (red triangles) in the space of source distance D_L and localization $\Omega_{50\%}$. Events which are not within the field of view in the 1 day time window are drawn with empty markers, while events which do at least partially overlap have solid markers. Three red crosses mark the events which pass the selection criteria for the short time window and also have an overlap with the field of fiew during that time. The shaded regions define the set of accepted events according to the selection citeria described in the text. The hatched region marks class I, which is solely relevant for the short analysis time window, and the solid regions mark classes II, III, and IV.

with a GW source originating from a primary photon from that source depends on multiple parameters, like the precise value of the Fisher discriminant, the direction of the source, and its localization quality.

As a first measure to limit the total background, two (mutually exclusive) time windows have been defined during which a GW source is analyzed. A short time window of $\Delta t_{\rm short} = 1000\,{\rm s}$ starting at $t_0 = -500\,{\rm s}$ before the GW event time, and a longer time window $\Delta t_{\rm long} = 1\,{\rm day}$ starting at $t_0 = +500\,{\rm s}$ after the GW event time have been chosen. While the short time window serves as a window for potential discovery with a high degree of sensitivity, the long time window is the result of a compromise between sensitivity and a long-term follow-up and is loosely motivated by the timescale predicted by Fang & Metzger (2017) for the emission of UHE neutrinos.

An analysis of the GW sky localization maps distributed by LIGO/Virgo leads to the conclusion that using their 50% contour, defining a solid angle $\Omega_{50\%}$, as the search region in the sky is a reasonable compromise between the expected level of background (which is proportional to the solid angle of the analyzed sky region) and the CL at which the true source is localized within the search region. By using the 50% contour instead of the 90% contour, which is the most commonly adopted convention, on average about 4 times as many GW sources may be analyzed before the same level of expected background is reached, while only losing 40% in confidence that the source is located within the analyzed sky region. To also take into account the directional resolution of the Auger SD, which is about 1° for photon-induced air showers above $10^{19}\,{\rm eV}$, the sky localization maps of GW sources are convolved with a corresponding Gaussian distribution before constructing the 50% contour.

In order to keep the sensitivity to a possible photon signal as high as possible, GW events are additionally selected by their localization quality and distance. Close and well-localized sources are preferred over distant and poorly localized ones. Thus, optimal results can be obtained while keeping the expected background at a reasonable level. Four classes of accepted GW events are defined here for which the 50% localization region is analyzed for coincident air-shower events (see Figure 2). These selection criteria can be summarized as

$$\begin{aligned}
(D_{\rm L} < \infty \text{ and } \Omega_{50\%} < 100\ {\rm deg}^2)_{\rm s} &\text{ “class I”}\\
(D_{\rm L} < \infty \text{ and } \Omega_{50\%} < 20\ {\rm deg}^2)_{\rm l} &\text{ “class II”}\\
(D_{\rm L} < 180\ {\rm Mpc} \text{ and } \Omega_{50\%} < 100\ {\rm deg}^2)_{\rm l} &\text{ “class III”}\\
(D_{\rm L} < 50\ {\rm Mpc} \text{ and } \Omega_{50\%} < 720\ {\rm deg}^2)_{\rm l,s} &\text{ “class IV”},
\end{aligned}$$

with the lowercase “l” and “s” in the subscript denoting in which time window (long and/or short) each class of events is analyzed.

The first class (class I) comprises GW sources with a maximum 50% contour size of $\Omega_{50\%} = \Omega_{\rm crit} = 100\,{\rm deg}^2$ and any distance. The value of $\Omega_{\rm crit}$ is chosen such that $\bar{P}_{\rm bg}$ for a photon candidate event within a 1000 s time window would always be above the 5σ level in this specific event (i.e., omitting any penalization factor from multiple trials). Since classically no photon signal is expected from very distant sources, this class also keeps a window open for potential discoveries of new physics. GW events in this class are analyzed only in the short time window.

Table 1
Summary of the 10 GW Events That Pass the Event Selection

	UTC Time	δ_{GW}	α_{GW}	D_L/Mpc	$\Omega_{50\%}$/deg^2	Source Type	Class	Time Window
GW150914	2015-09-14T09:50:45.4	$-72.^{\circ}7$	$-16.^{\circ}9$	429	73.6	BBH	I	short
GW170817	2017-08-17T12:41:04.4	$-23.^{\circ}4$	$-162.^{\circ}6$	41	3.1	BNS	all	long
GW170818	2017-08-18T02:25:09.1	$22.^{\circ}4$	$-18.^{\circ}7$	1033	15.7	BBH	I,II	long
GW190517_055101	2019-05-17T05:51:01.8	$-46.^{\circ}5$	$-130.^{\circ}9$	2270	83.6	BBH	I	short
GW190701_203306	2019-07-01T20:33:06.6	$-7.^{\circ}3$	$37.^{\circ}8$	2152	18.2	BBH	I,II	long
GW190728_064510	2019-07-28T06:45:10.5	$7.^{\circ}75$	$-46.^{\circ}5$	858	67.3	BBH	I	short
GW190814	2019-08-14T21:10:39.0	$-24.^{\circ}9$	$12.^{\circ}7$	241	7.8	BHNS	I,II	long
GW200208_130117	2020-02-08T13:01:17.9	$-33.^{\circ}7$	$139.^{\circ}4$	2258	13.8	BBH	I,II	long
GW200224_222234	2020-02-24T22:22:34.4	$-10.^{\circ}2$	$175.^{\circ}2$	1677	18.0	BBH	I,II	long
GW200311_115853	2020-03-11T11:58:53.4	$-6.^{\circ}6$	$1.^{\circ}6$	1152	16.2	BBH	I,II	long

Notes. The columns display (from left to right) the event identifier, the UTC time stamp of the GW detection by LIGO/Virgo, the decl. δ_{GW} and R.A. α_{GW} of the most likely source direction, the best estimate of the source luminosity distance D_L, the size $\Omega_{50\%}$ of the 50% contour of the GW localization map after its convolution with the directional reconstruction uncertainty, and the most likely source type: binary black hole merger (BBH), binary neutron star merger (BNS), or black hole-neutron star merger (BHNS). The last two columns indicate the classes in terms of $\Omega_{50\%}$ and D_L that apply to each event and the time window of the present analysis during which the 50% contour of the GW event was observed. For further information on the individual GW data, the reader may refer to the corresponding catalogs (Abbott et al. 2019, 2021a, 2021b, 2021c) published by the LIGO/Virgo collaborations and the associated public data release files (FITS files).

Especially well-localized sources with $\Omega_{50\%} \leqslant 20\,\mathrm{deg}^2$ are additionally analyzed in the long time window (class II). From such a small region in the sky, the expected background would still be small ($\bar{P}_{\mathrm{bg}} > 4\sigma$) despite the longer observation time, and the detection of a coincident photon-like event from a distant source could be a hint toward new physics.

The long time window is also applied to GW events in the third class (class III) that comprises sources with a maximum contour size of $100\,\mathrm{deg}^2$ which at the same time are required to be closer than 180 Mpc. The maximum distance is chosen such that we reject GW sources from which no photons are expected to reach the Earth even under the most optimistic assumptions about the photon flux and its emission pattern, unless new physics is involved. For this choice, a "photon horizon" h_γ has been estimated. This photon horizon is the distance up to which the energy transferred in to UHE by the so far brightest GW source, with a total radiated mass of almost $10\,M_\odot$, could be constrained to be less than its radiated GW energy. This distance is mainly driven by the photon attenuation length in the extragalactic medium. Using the CRPropa 3 simulation code (Batista et al. 2016) to simulate the propagation of UHE photons, a maximum horizon of $h_\gamma = 90$ Mpc has been found for photons at 10^{20} eV. This horizon is derived for isotropic emission. To take into account sources which might expose narrow jets pointing directly toward Earth, only sources beyond $D_L > 2h_\gamma$ are rejected.

A final class of accepted GW events (class IV) allows especially close sources to be analyzed up to a maximum allowed contour size of $720\,\mathrm{deg}^2$. For such sources with luminosity distance $D_L \leqslant 50$ Mpc, there is a realistic chance of observing a potential UHE photon flux or at least of placing strong physical constraints on the fraction of energy transferred into UHE photons. The value of 50 Mpc is defined by the maximum distance a source like GW170817 may have so that the fraction of energy transferred into UHE photons could still be constrained by a nonobservation of photons at the SD array. The cut on the maximum contour size is chosen such that the bulk of GW events would be accepted and only the tail (about 10%) in the distribution of $\Omega_{50\%}$ is rejected, which can mostly be addressed to events that were not observed by one of the two LIGO detectors.

The four classes are not mutually exclusive and, hence, a single GW event may belong to multiple classes at the same time. Although classes II and III are subsets of class I in the space of $\Omega_{50\%}$ and D_L, an event belonging, for example, to class II can only be analyzed in class I as well if its localization contour overlaps with the field of view during the short time window.

In Figure 2, the accepted regions in the space of source localization $\Omega_{50\%}$ and luminosity distance D_{L} are visualized on top of the distribution of all 91 confident GW observations detected between O1 and O3b. In total, 23 GW events qualify in terms of $\Omega_{50\%}$ and D_L for being checked in the short time window (classes I or IV), and a subset of eight for also being checked in the long time window (classes II−IV). Out of these 23 (eight) GW events, in three (seven) cases the localization contours were at least partly covered by the Auger SD field of view in the short (long) time window. The three events in the short time window belong exclusively to class I, i.e., none of these events also qualifies for an inspection in the long time window. All seven events in the long time window are found in class II. One of these, GW170817, also passes the selection criteria for classes I, III, and IV, but it was not observable in the short time window. For a quick reference, further information about the 10 GW events that pass the event selection, like the precise time stamp of their detection, the most likely source direction, the source distance and most likely source type, are compiled in Table 1. For a more comprehensive reference of the GW signals, one may refer to the official catalogs GWTC-1, GWTC-2, GWTC-2.1, and GWTC-3 published by the LIGO and Virgo collaborations.

5. Sensitivity

In view of the future growth of the GW data set, let us first consider the overall sensitivity of this analysis to a photon signal. As in Section 4, the sensitivity is quantified by adopting the photon candidate cut value of Abreu et al. (2023) and assuming a single photon candidate event within any of the sky regions and time windows analyzed here for the seven (three) events selected. While the expected number of random air showers (i.e., irrespective of the Fisher discriminant) to be coincident with any of the analyzed GW sources and time windows is about 0.03, the expected total background with a

Fisher discriminant value exceeding the cut value is $b = 9.1 \times 10^{-6}$ events. This leads to $\bar{P}_{\rm bg} = 4.44\sigma$, meaning that the hypothesis of such a photon candidate event belonging to the hadronic background could have been rejected at a CL of 4.44σ. Since this value is calculated for the combined background from all selected GW sources, in both the long and the short time windows, it naturally takes into account the trial factor that comes with an increasing number of analyzed sources. Considering future applications of this analysis to larger sets of GW sources, this penalized value of $\bar{P}_{\rm bg}$ is expected to decrease. The real value of $\bar{P}_{\rm bg}$ in the actual case of a coincident air-shower detection will, however, strongly depend on the precise values of the photon-discrimination observables $L_{\rm LDF}$ and Δ as well as the direction and photon energy of the event. These values carry more detailed information about the primary particle and its photon likeliness than the binary selection method that is introduced by a simple photon candidate cut.

6. Results

For both analysis time windows of 1000 s and 1 day the data of the Pierre Auger Observatory have been analyzed for possible coincident photon events. No coincident air showers with $E_\gamma > 10^{19}$ eV occured for any source in either of the time windows. This is well in agreement with the expected amount of 0.03 chance coincidences. Consequently, also none of the 16 photon candidate events from Abreu et al. (2023) was found to be coincident with any of the selected GWs. Following this nonobservation of coincident events, for each GW source an upper limit on the number of photons can be placed using the FC approach. In general, the FC upper limit at 90% CL without a measured signal and zero background is $N_\gamma^{\rm UL} \approx 2.44$. The small amount of background which is expected, however, does not significantly change this number.

From $N_\gamma^{\rm UL}$, one can obtain limits on the corresponding spectral photon flux $\frac{d\Phi_\gamma^{\rm GW}}{dE_\gamma}(E_\gamma)$, which is the number of photons arriving at the Earth from the direction of the GW source per unit time and area in the energy range $[E_\gamma,\ E_\gamma + dE_\gamma)$. Assuming that the spectral photon flux follows a power law with spectral index α, it can be written as

$$\frac{d\Phi_\gamma^{\rm GW}}{dE_\gamma}(E_\gamma) = k_\gamma E_\gamma^{\alpha}. \tag{1}$$

With the energy dependence of the flux modeled as a power law, an upper limit on the flux normalization factor $k_\gamma^{\rm UL}$ can be derived from $N_\gamma^{\rm UL}$ as

$$k_\gamma^{\rm UL} = \frac{N_\gamma^{\rm UL}}{\int_{E_0}^{E_1} dE_\gamma E_\gamma^{\alpha}\, \mathcal{E}(E_\gamma,\, \theta_{\rm GW},\, \Delta t)}. \tag{2}$$

For comparison to other results, the energy interval $[E_0,\ E_1)$ covers one order of magnitude starting with 10^{19} eV. $\mathcal{E}(E_\gamma,\, \theta_{\rm GW},\, \Delta t)$ is the directional exposure of the Observatory to photons with energy E_γ within the time interval $\Delta t = t_1 - t_0$. The calculation of $\mathcal{E}$ is explained in the following.

The quality cuts that are imposed on the Auger SD data (see Section 2) limit the photon detection efficiency as a function of the energy and zenith angle of the incident primary particle. The zenith-angle-averaged photon efficiency between 30° and 60° and $E_\gamma > 10^{19}$ eV, assuming an E_γ^{-2} power spectrum, has been found to be $\epsilon \simeq 0.54$. The efficiency has been derived using simulated photon events produced with the CORSIKA simulation code (Heck et al. 1998) and after applying the same selection cuts as used for data. With the photon efficiency given as a function of energy and direction, the exposure to UHE photons from a transient point source at zenith angle $\theta_{\rm GW}$ during the obervation period between t_0 and t_1 is given by

$$\mathcal{E}(E_\gamma,\, \theta_{\rm GW},\, \Delta t) = \int_{t_0}^{t_1} dt\, A(t)\, \epsilon\,(E_\gamma,\, \theta_{\rm GW}) \times \Theta_{\rm FoV}(\theta_{\rm GW}(t))\, \cos(\theta_{\rm GW}(t)), \tag{3}$$

with $A(t)$ being the time-dependent effective area of the Auger SD array, which is determined by the number of active SD stations at a given moment. The step function $\Theta_{\rm FoV}$ accounts for the fraction of the observation time in which the source is covered by the field of view of the SD between zenith angles of 30° and 60°. Since the zenith angle $\theta_{\rm GW}$ of a GW source is a coordinate of the horizontal coordinate system which corotates with the Earth, $\theta_{\rm GW}$ is a function of the sidereal time t, source R.A. $\alpha_{\rm GW}$, and decl. $\delta_{\rm GW}$:

$$\cos(\theta_{\rm GW}(t)) = \sin\lambda \sin\delta_{\rm GW} + \cos\lambda \cos\delta_{\rm GW} \sin(2\pi t/T - \alpha_{\rm GW}), \tag{4}$$

with λ being the latitude of the Auger SD array and T the duration of a sidereal day. After weighting the exposure by a E^{-2} spectrum and integrating over a decade in energy, the spectrum-weighted exposure $\bar{\mathcal{E}}$ is a function of source R.A. and decl. during the short time window, while in the long time window $\bar{\mathcal{E}}$ depends only on decl. to first order and is depicted by the dotted curve in Figure 3. The exposure has a maximum at the celestial pole and vanishes for $\delta_{\rm GW} > 24.6°$. The basic structure of the exposure curve is determined by the visibility of a certain direction in the zenith band between 30° and 60° modulated by the directional photon detection efficiency ϵ. For each GW source analyzed in the long time window, the decl.

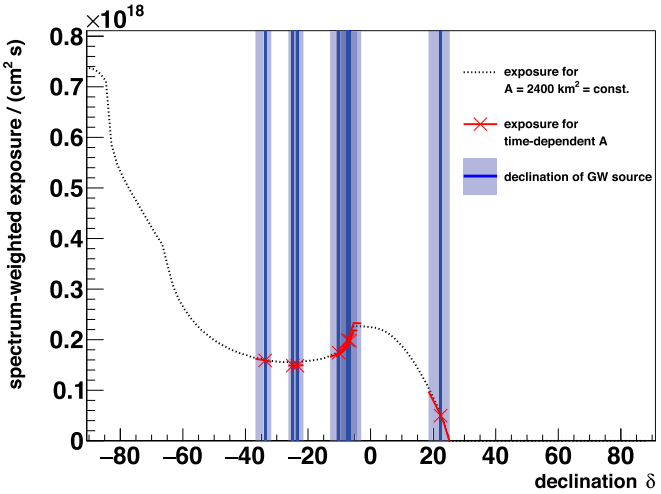

Figure 3. The spectrum-weighted exposure as a function of source decl. for a benchmark effective area of the SD array of 2400 km^2 (dotted curve). The decl. ranges covered by the 50% localization regions of the seven GW events selected in the long time window are marked by the shaded bars, with the most likely source directions marked by the dark blue bars. For each GW event the actual exposure, taking into account the time-dependent effective area of the SD in the long time window, is indicated by the red lines.

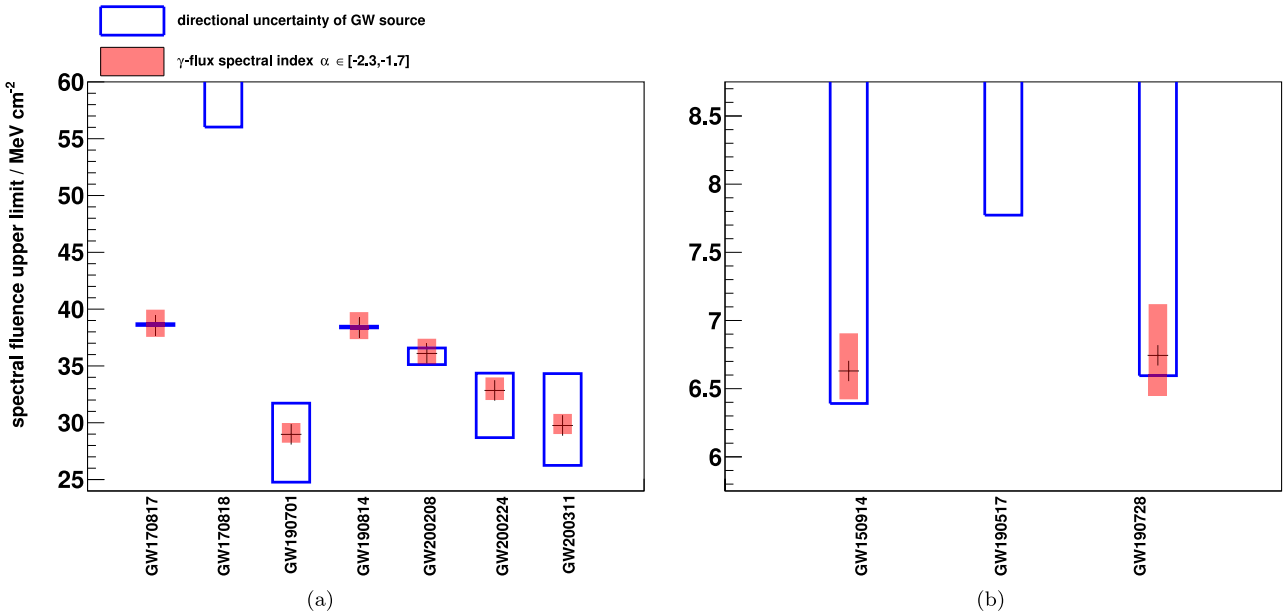

Figure 4. Upper limits (at 90% CL) on the spectral fluence of UHE photons from the selected GW sources for the searches in (a) the long and (b) the short time window. The limits for the most likely direction and a spectral index of $\alpha = -2$ are marked by the cross. The blue (empty boxes) error bars correspond to the variation of the upper limits due to the directional uncertainty of the source. Red (shaded boxes) error bars show the impact of a variation of the spectral index. For contours which are partly outside the field of view, the blue error bars grow to infinity (e.g., in the case of GW170818). While in the case of GW170818 in (a), the most likely direction is close to the edge of the field of view, yielding a large upper limit of 109 MeV cm^{-2}, no limit could be placed on the most likely direction of GW190517 in (b) as it was not inside the observed zenith-angle range during the short time window.

band covered by the $\Omega_{50\%}$ contour is highlighted in Figure 3 by a blue shaded bar, with the most likely source decl. marked with a solid line. Since the effective area A of the SD array varies over time (typically only at the percent level), the actual time-dependent values of the exposure are highlighted in solid red next to the dotted benchmark line, which is based on a fixed area of 2400 km^2 corresponding to a typical average value.

Finally, an upper limit on the spectral fluence $\mathcal{F}_\gamma^{\rm UL}$ of UHE photons arriving from a given source at the Earth can be derived from the flux upper limit:

$$\mathcal{F}_\gamma^{\rm UL} = \int_{t_0}^{t_1}\int_{E_0}^{E_1} dt\, dE_\gamma\, E_\gamma\, \frac{d\Phi_\gamma^{\rm GW}}{dE_\gamma}. \quad (5)$$

While no assumption on the time dependence of the flux is made, the extrapolation of the flux limits (which are based on data while the source is in the field of view) to the full time window implicitly assumes that the average flux during the period for which the source has been in the field of view is representative of the whole time window. The limits on the spectral fluence depend on the exact direction of the GW source and change with a variation of the assumed spectral shape of the UHE photon flux. Hence, in Figure 4 the results for $\mathcal{F}_\gamma^{\rm UL}$ are shown for all possible source directions within each localization contour and a variation of the spectral index $\alpha \in [-2.3, -1.7]$ for both time windows. In the long time window, all localization regions have been fully covered by the field of view except for GW170818. Hence, this event could not be constrained for all source directions within the $\Omega_{50\%}$ contour. All three GW sources in the short time window have contours which partly leak out of the field of view. The upper limits that could be placed in the long (short) time window vary typically around $\sim$35 MeV cm^{-2} ($\sim$7 MeV cm^{-2}).

The BNS merger GW170817 plays a special role in this analysis for multiple reasons: as the first GW source which has a confirmed observation of an electromagnetic counterpart, a kilonova (Arcavi et al. 2017), the BNS merger is especially interesting for all kinds of follow-up multimessenger studies. So far, this source is also the only GW source for which the host galaxy has been identified, in this case NGC 4993 at a distance of about 41.0 ± 3.1 Mpc (Hjorth et al. 2017). This makes GW170817 the closest and best localized source to date. While a large fraction of a potential UHE photon flux from NGC 4993 is expected to be attenuated by the cosmic background radiation fields, the intergalactic medium still has a degree of transparency to UHE photons and first constraints on the energy transferred into UHE photons can be derived. To accurately take into account the interactions of photons, the photon attenuation has been studied as a function of photon energy using CRPropa 3. The upper limit to the spectral fluence at Earth $\mathcal{F}_\gamma^{\rm UL}$, with an underlying flux modeled according to an E^{-2} power-law spectrum, is then back-propagated to the source of the BNS and extrapolated to a full sphere to gain a limit on the energy transferred into UHE photons. Upper limits that do not exceed the GW energy lower limit of $E_{\rm GW} \gtrsim 0.04\ M_\odot$ can be placed for photons above 2×10^{19} eV. Furthermore, we find that the strongest limits can be placed for photon energies above 4×10^{19} eV, where less than 20% of the total GW energy at 90% CL is transferred into UHE photons. Since the attenuation of UHE photons follows an exponential law, this result indicates that the energy transferred into UHE photons by an even closer GW source, which might be observed in the near future, could likely be constrained well below the percent level.

7. Conclusion

With the large exposure of its surface detector array, the Pierre Auger Observatory has been utilized to investigate a

possible outflow of UHE photons from the GW sources detected in recent years. The focus of this study was photons with energies above 10^{19} eV. Searching for transient point sources of photons at such energies comes with two major difficulties: the attenuation of UHE photons in the cosmic background radiation fields, which reduces the photon interaction length to only a few megaparsecs, and the separation of primary photons from an overwhelming background of hadronic cosmic rays using air-shower properties. To overcome these obstacles, an educated selection of GW sources has been defined, aiming to maximize the physics impact of the results. These—in total 10—sources were analyzed for a coincident photon signal in a time span ranging from 500 s before the GW until one sidereal day after. Following the nonobservation of a coincident signal, limits on the spectral fluence of photons in the respective energy range were constructed assuming an E_γ^{-2} power-law spectrum. These are the first limits on UHE photons from GW sources.

The limits on the BNS merger GW170817 add one further piece to the overall multimessenger puzzle by constraining the electromagnetic outflow of the source in the UHE regime. The results can be compared to the observed fluence of gamma-rays between 50 and 300 keV as measured, for example, by the Fermi Gamma-ray Burst Monitor (Meegan et al. 2009) to be $(2.8 \pm 0.2) \times 10^{-7}$ erg cm^{-2} (Goldstein et al. 2017), which are more than two orders of magnitude stronger than the upper limits found here in the long time window (after extrapolating the limits to a comparable range in $\log(E)$). The results can also be compared to the limits on the photon flux between 4 and 100 TeV placed by the High-Altitude Water Cherenkov Observatory (HAWC; Abbott et al. 2017; Abeysekara et al. 2017) and on the fluence of neutrinos between 100 TeV and 1 PeV placed by IceCube (Aartsen et al. 2017; Albert et al. 2017). After converting our limits to a comparable range in $\log_{10}(E)$, we find that the limits placed in this work are of the same order of magnitude as the limits by HAWC by a factor of $\sim$2.6 weaker, and by a factor of $\sim$30 stronger than the neutrino limits by IceCube. In the case of HAWC, the comparable sensitivity of the observatories is mainly due to the exposure of the SD being compensated by the higher expected particle flux at lower energies and HAWC's larger field of view, covering almost 2π sr. The difference to the IceCube sensitivity additionally depends to a large extent on the different detection efficiencies between photons and neutrinos.

With the upcoming GW observation run O4, starting prospectively in 2023, a further increase in the detection rate is expected. With many more GW events to be analyzed in the future, a coincident air shower from the cosmic ray background will be almost certain at some point. Then, the photon likeliness of a coincident shower may be analyzed using dedicated simulations of photon-induced air showers aiming to mimic the signal found in the data. Comparing the Fisher discriminant of a coincident shower with the distributions obtained from photon simulations and hadronic background events, one can then judge the overall photon likeliness of the air shower on an event-by-event basis.

This analysis is only a first step toward exploiting the full potential of the Pierre Auger Observatory in multimessenger astronomy of transient point sources with UHE photons. While its sensitivity is already competitive with that of other instruments measuring photons and neutrinos at lower energies, the case of GW170817 shows the potential of the observatory if even closer GW sources should be detected in upcoming observation runs. A future observation of, for example, a BNS merger in the Virgo cluster of galaxies could possibly lead to a probe of the energy transferred into UHE photons at a level well below 1% of its GW energy, a significant improvement compared to the 20% $E_{\rm GW}$ obtained in this work for GW170817.

Acknowledgments

The successful installation, commissioning, and operation of the Pierre Auger Observatory would not have been possible without the strong commitment and effort from the technical and administrative staff in Malargüe. We are very grateful to the following agencies and organizations for financial support.

Argentina—Comisión Nacional de Energía Atómica; Agencia Nacional de Promoción Científica y Tecnológica (ANPCyT); Consejo Nacional de Investigaciones Científicas y Técnicas (CONICET); Gobierno de la Provincia de Mendoza; Municipalidad de Malargüe; NDM Holdings and Valle Las Leñas; in gratitude for their continuing cooperation over land access; Australia—the Australian Research Council; Belgium—Fonds de la Recherche Scientifique (FNRS); Research Foundation Flanders (FWO); Brazil—Conselho Nacional de Desenvolvimento Científico e Tecnológico (CNPq); Financiadora de Estudos e Projetos (FINEP); Fundação de Amparo à Pesquisa do Estado de Rio de Janeiro (FAPERJ); São Paulo Research Foundation (FAPESP) grant Nos. 2019/10151-2, 2010/07359-6, and 1999/05404-3; Ministério da Ciência, Tecnologia, Inovações e Comunicações (MCTIC); Czech Republic—grant Nos. MSMT CR LTT18004, LM2015038, LM2018102, CZ.02.1.01/0.0/0.0/16_013/0001402, CZ.02.1.01/0.0/0.0/18_046/0016010, and CZ.02.1.01/0.0/0.0/17_049/0008422; France—Centre de Calcul IN2P3/CNRS; Centre National de la Recherche Scientifique (CNRS); Conseil Régional Ile-de-France; Département Physique Nucléaire et Corpusculaire (PNC-IN2P3/CNRS); Département Sciences de l'Univers (SDU-INSU/CNRS); Institut Lagrange de Paris (ILP) grant No. LABEX ANR-10-LABX-63 within the Investissements d'Avenir Programme grant No. ANR-11-IDEX-0004-02; Germany—Bundesministerium für Bildung und Forschung (BMBF); Deutsche Forschungsgemeinschaft (DFG); Finanzministerium Baden-Württemberg; Helmholtz Alliance for Astroparticle Physics (HAP); Helmholtz-Gemeinschaft Deutscher Forschungszentren (HGF); Ministerium für Kultur und Wissenschaft des Landes Nordrhein-Westfalen; Ministerium für Wissenschaft, Forschung und Kunst des Landes Baden-Württemberg; Italy—Istituto Nazionale di Fisica Nucleare (INFN); Istituto Nazionale di Astrofisica (INAF); Ministero dell'Istruzione, dell'Universitá e della Ricerca (MIUR); CETEMPS Center of Excellence; Ministero degli Affari Esteri (MAE); México—Consejo Nacional de Ciencia y Tecnología (CONACYT) No. 167733; Universidad Nacional Autónoma de México (UNAM); PAPIIT DGAPA-UNAM; The Netherlands—Ministry of Education, Culture and Science; Netherlands Organisation for Scientific Research (NWO); Dutch national e-infrastructure with the support of SURF Cooperative; Poland—Ministry of Education and Science, grant No. DIR/WK/2018/11; National Science Centre, grant Nos. 2016/22/M/ST9/00198, 2016/23/B/ST9/01635, and 2020/39/B/ST9/01398; Portugal—Portuguese national funds and FEDER funds within Programa Operacional Factores de Competitividade through Fundação para a Ciência e a Tecnologia (COMPETE); Romania—Ministry of Research, Innovation and Digitization,

CNCS/CCCDI UEFISCDI, grant Nos. PN19150201/16N/2019 and PN1906010 within the National Nucleus Program, and projects number TE128, PN-III-P1-1.1-TE-2021-0924/TE57/2022 and PED289, within PNCDI III; Slovenia—Slovenian Research Agency, grant Nos. P1-0031, P1-0385, I0-0033, and N1-0111; Spain—Ministerio de Economía, Industria y Competitividad(FPA2017-85114-P and PID2019-104676GB-C32), Xunta de Galicia (ED431C 2017/07), Junta de Andalucía (SOMM17/6104/UGR, P18-FR-4314) Feder Funds, RENATA Red Nacional Temática de Astropartículas (FPA2015-68783-REDT) and María de Maeztu Unit of Excellence (MDM-2016-0692); USA—Department of Energy, Contract Nos. DE-AC02-07CH11359, DE-FR02-04ER41300, DE-FG02-99ER41107, and DE-SC0011689; National Science Foundation, grant No. 0450696; The Grainger Foundation; Marie Curie-IRSES/EPLANET; European Particle Physics Latin American Network; and UNESCO.

References

Aab, A., Abreu, P., Aglietta, M., et al. 2015, NIMPA, 798, 172
Aab, A., Abreu, P., Aglietta, M., et al. 2016, PhRvD, 94, 122007
Aab, A., Abreu, P., Aglietta, M., et al. 2017a, JCAP, 2017, 009
Aab, A., Abreu, P., Aglietta, M., et al. 2017b, ApJ, 837, L25
Aartsen, M., Ackermann, M., Adams, J., et al. 2017, JInst, 12, P03012
Abbott, B. P., Abbott, R., Abbott, T. D., et al. 2016, PhRvL, 116, 061102
Abbott, B. P., Abbott, R., Abbott, T. D., et al. 2017, ApJ, 848, L12
Abbott, B. P., Abbott, R., Abbott, T. D., et al. 2019, PhRvX, 9, 031040
Abbott, R., Abbott, T. D., Abraham, S., et al. 2021a, PhRvX, 11, 021053
Abbott, R., Abbott, T. D., Acernese, F., et al. 2021b, arXiv:2108.01045
Abbott, R., Abbott, T. D., Acernese, F., et al. 2021c, arXiv:2111.03606
Abeysekara, A. U., Albert, A., Alfaro, R., et al. 2017, ApJ, 843, 39
Abreu, P., Aglietta, M., Albury, J. M., et al. 2022, ApJ, 933, 125
Abreu, P., Aglietta, M., Allekotte, I., et al. 2023, JCAP, 05, 021
Albert, A., André, M., Anghinolfi, M., et al. 2017, ApJ, 850, L35
Arcavi, I., Hosseinzadeh, G., Howell, D. A., et al. 2017, Natur, 551, 64
Batista, R. A., Dundovic, A., Erdmann, M., et al. 2016, JCAP, 2016, 038
Decoene, V., Guépin, C., Fang, K., Kotera, K., & Metzger, B. 2020, JCAP, 2020, 045
Fairbairn, M., Rashba, T., & Troitsky, S. 2011, PhRvD, 84, 125019
Fang, K., & Metzger, B. D. 2017, ApJ, 849, 153
Feldman, G. J., & Cousins, R. D. 1998, PhRvD, 57, 3873
Galaverni, M., & Sigl, G. 2008, PhRvL, 100, 021102
Goldstein, A., Veres, P., Burns, E., et al. 2017, ApJ, 848, L14
Gorski, K. M., Hivon, E., Banday, A. J., et al. 2005, ApJ, 622, 759
Heck, D., Knapp, J., Capdevielle, J. N., Schatz, G., & Thouw, T. 1998, Forschungszentrum Karlsruhe Report FZKA 6019, College de France, Paris
Hjorth, J., Levan, A. J., Tanvir, N. R., et al. 2017, ApJ, 848, L31
Kampert, K.-H., Mostafa, M. A., Zas, E., Pierre Auger Collaboration, et al. 2019, FrASS, 6
Kimura, S. S., Murase, K., & Mészáros, P. 2018, ApJ, 866, 51
Kotera, K., & Silk, J. 2016, ApJ, 823, L29
McKernan, B., Ford, K. E. S., Bartos, I., et al. 2019, ApJ, 884, L50
Meegan, C., Lichti, G., Bhat, P. N., et al. 2009, ApJ, 702, 791
Murase, K., Kashiyama, K., Mészáros, P., Shoemaker, I., & Senno, N. 2016, ApJ, 822, L9
Risse, M., & Homola, P. 2007, PhL, 22, 749
Rodrigues, X., Biehl, D., Boncioli, D., & Taylor, A. 2019, APh, 106, 10